RSC Advances

ROYAL SOCIETY OF CHEMISTRY

www.rsc.org/advances

RSC Advances ARTICLE
www.rsc.org/advances

$Y_2BaZnO_5:Er^{3+}$ microcapsules with enhanced upconversion by vanadium ion codoping

Hom Nath Luitel*, Rumi Chand, Toshio Torikai, Mitsunori Yada, Takanori Watari#

Received () Xth XXXXXXXXX 20XX, Accepted Xth XXXXXXXXX 20XX
DOI:

Microcapsules of $Y_2BaZnO_5:Er^{3+}$ nanocrystals were successfully prepared by a simple hydrothermal method using citric acid as chelating agent. The sizes of the spherical microcapsules were varied between 1-5 μm with wall thickness of about 50-100 nm. The underlined microcapsule formation mechanism was discussed using gas-bubble-assisted Ostwald ripening process. The $Y_2BaZnO_5:Er^{3+}$ microcapsules exhibited characteristic upconversion (UC) emissions of Er^{3+} with intense yellowish orange color under dual laser pumping at 808 nm as well as 980 nm. Concentration dependent studies revealed that the optimum Er^{3+} concentration for intense UC at 550 nm and 660 nm were 5 mol% and 7 mol%, respectively. In addition, the optimum Er concentration differed from the excitation wavelength indicating different UC mechanism. Importantly, optimum amount of the V^{5+} co-doping into the $Y_2BaZnO_5:Er^{3+}$ phosphors intensified the UC intensity by more than 3 fold. The $Y_2BaZnO_5:Er^{3+},V^{5+}$ phosphor exhibited intense yellowish UC pumped by 808 nm laser and will have potential applications for the in vivo biological labelling, biomedical imaging and therapies.

1. Introduction

Upconversion is a process in which two or more low-energy photons are converted to a single high-energy photon. Various processes can lead to upconversion, including two/three/multiple-photon absorptions, ground state followed by excited state absorption, energy transfer upconversion, second harmonic generation, and photon avalanche [1,2]. Since its discovery in the 1960s, upconversion (UC) has been the focus of many researchers [2–5]. These UC materials with strong luminescence in the NIR to visible to near UV region has been extensively investigated in recent years due to their several potential applications in solar cells [3], novel 3D display technologies [2,6,7], inks for secure printing [8], optical communication and amplifiers [9,10], high density optical storage [2], infrared detection and sensors [11], and more recently bio medical labelling, imaging and therapies [4,12,13].

Lanthanide ions are often employed as UC luminescence centres due to the abundant energy states of 4f configurations in Ln^{3+} ions and hence the UC emission proceed via various excited state absorption (ESA) and energy transfer (ET) pathways. Among the various lanthanide ions, Er^{3+}, Ho^{3+}, Tm^{3+}, Nd^{3+} and Pr^{3+} were studied for UC luminescence [9,13–17]. However, there are very limited f–f transitions from ground state of these RE^{3+} ions whose energy matches the energy of the excited photons, thus the ground state absorption (GSA) of these ions is extremely poor. The Yb^{3+} is the most commonly used sensitizer in UC luminescence to harvest pump photons and subsequently promotes neighbouring activator ions (like Er^{3+}) to the excited states because of its wider absorption cross-section around 980 nm, simple two-level structure ensuring its very high quenching concentration and large spectral overlap (Yb^{3+}; $^2F_{5/2}$ to $^2F_{7/2}$) with Er^{3+} absorption ($^5I_8$ to $^5I_6$) which ensures efficient energy transfer from Yb^{3+} to Er^{3+} and other RE^{3+} ions [4,6,9]. Thus, UC luminescence of RE^{3+} in RE^{3+}/Yb^{3+} co-doped systems have been extensively studied, and predominant green to red UC emissions have been obtained, especially in low phonon energy hosts, such as fluoride [18,19], garnets [9,16], sulfide and oxy-sulfide [16,20] and glasses [9,19].

For bio-imaging and therapies, nanoparticles with high brightness with continuous emission are desired. In addition, they should be resistant to photo-bleaching. Lots of effort has been made to utilize $NaYF_4:Er^{3+}$ for bioimaging and therapies [2,4,12,21,22]. However, they suffer severely due to high toxicity, low sensitivity, and low penetration depth of 980 nm laser in the body tissue, since the excellent optical window of the body tissue is 700-900 nm [23]. Importantly, present upconversion nanoparticles (UCNP) suffer badly due to their low efficiency [20]. In UC based techniques, detection sensitivity depends on the luminescence intensity of the phosphor. Recently, several attempts in case of UCNPs have been made to increase the luminescence intensity, such as codoping with sensitizer ions [9,14,24], crystal surface coating [2,25], core/shell synthesis [26], *etc.*, but most of them are not enough to improve the UC intensity to desire level (should be pumped by as low as 1 mW laser power to protect human tissue from burning by laser heat). Hence, the luminescence intensity enhancement of UCNPs is still a challenging topic.

Compared to the huge number of studies on the $NaYF_4$:Yb,Er nanocrystals, very small effort has been paid on the work of oxide based UC phosphors [9–11,13–15,17,19,20,24,27]. Moreover, the study of 808 nm excited visible UC luminescence has not been in focus despite most suitable spectral range for the bioimaging and therapies due to best match of optical window of body tissue (700-900 nm). We have previously reported efficient oxide based NIR to NIR upconversion phosphor ($CaMoO_4$:Tm,Yb,K) pumped by 980 nm laser [28]. However, the 980 nm laser has low penetration depth compared to the 808 nm laser. Thus, in this paper we present efficient dual NIR laser (808 nm and 980 nm) pumped VIS UC emission in an oxide based sub micrometer phosphor, $Y_2BaZnO_5:Er^{3+}$. Further, V^{5+} co-dopant has been identified first time for the enhancement of the UC intensity of Er^{3+} ions. Luminescence and absorbance measurements were reported for a series of Er^{3+}-doped and Er^{3+}, V^{5+} co-doped nanocrystalline microcapsules to achieve the highest UC intensity and to provide insight in the mechanism responsible for the UC luminescence.

2. Experimental

2.1 Sample preparation

Y_2BaZnO_5 phosphor doped with Er^{3+} and/or V^{5+}/Yb^{3+} ions were prepared by a simple hydrothermal (HT) process. In a typical hydrothermal reaction, 10 mM mixture of metal ions *viz.* Y, Ba, Zn, RE and/or Yb, V ($Y(NO_3)_3.6H_2O$, $Ba(NO_3)_2$, $Zn(NO_3)_3.6H_2O$, $Er(NO_3)_3.5H_2O$, $Yb(NO_3)_3.5H_2O$, NH_4VO_3) were prepared in a beaker with distilled water by constant stirring with magnetic stirrer. Citric acid was used as chelating agent (total metal ions to citric acid ratio was fixed to 4:1) and urea as precipitating agent (total metal ions to urea was fixed to 1:40). The pH of the resulting solution was adjusted by aqueous ammonia/nitric acid. 30 ml of the mixture was poured into a 50 ml Teflon lined stainless steel autoclave and kept at

120 ℃ for 12 hours. The white solid obtained was centrifuged, washed multiple times with distilled water followed by ethanol and freeze dried for 12 h. Each sample was further calcined at 700~1200 ℃ for 3 h to get the final highly crystalline $Y_2BaZnO_5:Er^{3+}$ phosphor.

2.2 Characterizations

Phase identification was carried out using a Shimadzu XRD-6300 instrument with Cu Kα radiation. The morphology of the phosphor particles were characterized by scanning electron microscopy (Hitachi-S3000N). Elemental analysis and mass percentage of the constituent ions were estimated using EDX coupled with SEM. Before SEM measurements, each sample was coated roughly 5 nm in thickness with platinum-palladium using Hitachi E-1030 ion sputter. Precise elemental analysis for the powder sample was carried out using Rayny EDX-800HS energy dispersive X-ray fluorescence spectrometer. The upconversion (UC) emission spectra, pumped by 808 nm and/or 980 nm cw laser (≤1-200 mW output power) were recorded using USB 4000 UV-VIS-NIR miniature fiber optic spectrometer (Ocean optics). Absorbance spectra were recorded using Shimadzu 6545 UV-VIS-IR spectrometer using integration sphere mounting the sample in quartz slides. All measurements were carried out at room temperature unless specified.

3. Results and discussion

Figure 1(a) presents the phase analysis of Y_2BaZnO_5 doped with different moles of Er^{3+} ions. The XRD patterns of all the samples agree very well with the Y_2BaZnO_5 standard JCPDS pattern (52-1688) and no distinguished secondary phases were identified. The Y_2BaZnO_5 consists of orthorhombic crystal structure with P*nmb* space group as depicted in Fig. 1(b). Further, isotropic substitution by Er^{3+} (and Yb^{3+}) in to the Y^{3+} sites did not altered the Y_2BaZnO_5 phase. Cell parameters obtained from the XRD data of the typical sample (3 mol% Er doped Y_2BaZnO_5) were; a = 7.068 Å, b = 5.705 Å and c = 12.334 Å, slightly smaller than the reported data of pure host [JCPDS:52-1688], which is attributed to the slightly smaller ionic radii of the Er^{3+} (0.100 nm) compared to the host ion Y^{3+} (0.102 nm) [29]. Very similar XRD patterns without distinguished impurity was observed by co-doping with various Yb^{3+} moles as shown in supporting materials.

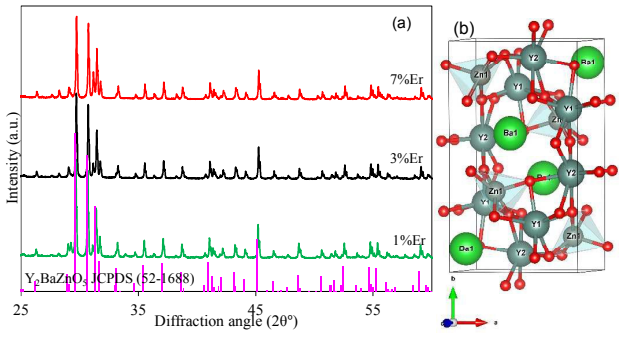

Fig.1 (a) XRD patterns of various moles of Er^{3+} substituted $Y_2BaZnO_5:Er^{3+}$ phosphors and (b) crystal structure created by VISTA program.

Figure 2 reveals the morphology of various Y_2BaZnO_5:0.03Er phosphor particles as prepared hydrothermally at 120℃ for 12 h as well as under heat treated at 1000℃. The SEM images revealed that almost mono-dispersed microcapsules of size between 1 to 5 µm were obtained. A closer look of the SEM images as shown in the Fig. 2(b, c) suggested that the microcapsules are really hollow with wall thickness ranging between 50-200 nm (see supporting Fig. S1 for detail). The wall of the micro-capsules consisted of nanoparticles of size between 30-100 nm. Further, some non-oriented nanograins were observed whose particles dimensions varied between some tens of nanometres up to 200-300 nm as shown in Fig. 2(d). It is important to state that the microcapsules were stable up to relatively high temperatures, ~1000℃ as shown in Fig. 2(e) and the supporting Fig. S2. During the thermal treatment process, the size of the microcapsules slightly reduced, but the capsular shape remained intact. However, further increase of sintering temperatures above 1000 ℃ destroyed the microcapsules and formed agglomerated nanoparticles as shown in Fig. S2. The EDX spectrum of the selected surface of microcapsules (Fig. 2(f)) proved that the microcapsules really consisted of Y_2BaZnO_5 phase. Further, precise compositional analyses were carried out using X-ray fluorescence spectroscopy (see supporting information S4 for the mass composition). The elemental compositions confirmed that the doped ions, especially Er, Yb and V were really incorporated in to the Y_2BaZnO_5 matrix.

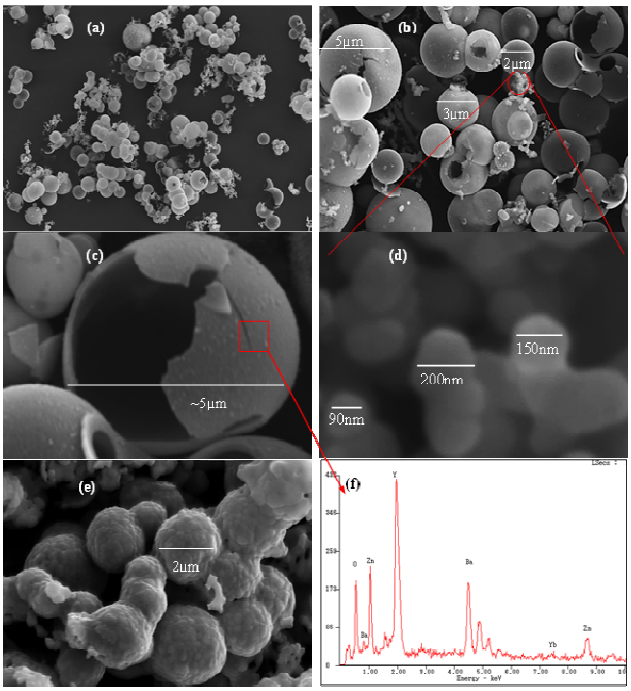

Fig. 2. SEM images of Y_2BaZnO_5:0.03Er hollow shperes as prepared hydrothermally at 120 ℃ for 12 h under different magnifications (a, b, c, d), sample (a) heat treated at 1000℃ for 3 h (e), and EDX spectra of selected area (f).

Under, these experimental results, the formation mechanism of those microcapsules can be outlined by gas-bubble-assisted Ostwald ripening through self templated, self-assembly process as shown in the scheme of Fig.3 [30]. First, citric acid dissolved in the solution and citrate anions were formed. Then the metal ions get complexes with the citrate molecules and controlled precipitation through hydrolysis forms crystal nuclei or nanograins. As the reaction progress, the nanograins have tendency to aggregate to minimize the total surface energy. Thus, at high temperature hydrothermal treatment process, nanograins begin to aggregate via an Ostwald ripening process and form the aggregated structures [31]. During the hydrothermal treatment at high pressure, these aggregates roll over smoothly and form spherical balls. During the progress of the HT treatment time, more nanograins self-assemble on to the surface of the sphere to minimize the total surface energy and bigger spheres are expected. Here, each sphere acts as a template for nanograins formed from the same sphere itself. This Ostwald ripening and gas-bubble-assisted-assembly process going on, more and more nanograins attached on the surface of the sphere and bigger balls are

formed. The spherical, somehow solid or semi solid spheres as depicted in the supporting information S3 (b, b-1) can be well explained by above mention mechanism. However, if excess urea (metal ions/urea = 1/40) was used, microcapsules with hollow architectures were formed as depicted in Fig. 2 and supporting information S3 (a, a-1). As mentioned by Liu et al. [30], when excess urea is used during the HT treatment process, ammonia/N_2 gas-bubbles were continuously generated. These gas-bubbles provide aggregation centres for nanograins and gas-bubble-nanograins aggregates are formed as shown in scheme in Fig. 3. Here, the citrate ions acts as surfactants and inhibits the hydrolysis of the metal cations used in the reactions (here, Zn^{2+}, Ba^{2+}, Y^{3+}, RE^{3+}) and facilitates the slow growth of the nanoparticles, otherwise nanograins agglomerates rapidly and forms irregular solids. Further, citrate ions increased the viscosity of the HT solution. At viscus solution, stabilized gas-bubbles form regular hollow cores. Further, slow precipitation and movement rate of nanograins in viscus solution allow enough time to form regular spheres. This Ostwald ripening and gas-bubble-assisted-assembly process going on, more and more nanograins attached on the surface of the sphere and bigger balls with thicker wall are formed as shown in the supporting Fig S3 (a, a-1). A similar Ostwald self-assembled, self-templated process of CeO_2, ZnO and Al_2O_3 spheres formation has been reported in gas-bubble free conditions [31-34]. The size of the microcapsules, void size are expected to change according to the air-bubble size whereas the wall thickness are expected to control according to the HT reaction time and concentration of the citrate anions (rate of metal ions hydrolysis). The core size of the microcapsules varied remarkably in our results due to formation of different sizes air-bubbles. The air-bubble size could be control according to the citrate concentration (viscosity of the solution) and rate of bubbles formation (concentration of urea) and underlined phenomena are being carried out and expected to publish elsewhere in near future.

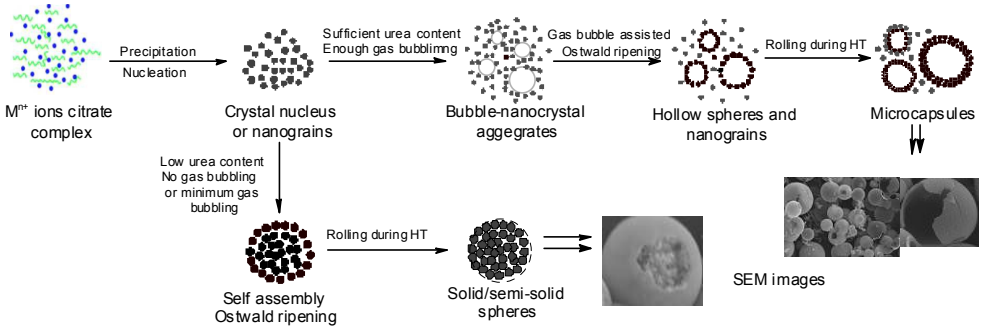

Fig.3 Schematic illustration of the formation mechanism of Y_2BaZnO_5:Er microcapsules by gas-bubble-assisted Ostwald ripening.

The UC emission phenomena of the Er^{3+} and Er^{3+} codoped with Yb^{3+} were studied by 808 nm as well as 980 nm laser excitation at room temperature and results are presenmted in Fig. 4. Y_2BaZnO_5:Er phosphors exhibited green emission centered around 520-560 nm corresponding to the ($^2H_{11/2}$, $^4S_{3/2}$ → $^4I_{15/2}$) electronic transition and comparatively stronger orange emission band centered around 650 nm corresponding to the ($^4I_{9/2}$ → $^4I_{15/2}$) electronic transition of Er^{3+} ion. With increasing Er concentration, both the 808 nm pumped as well as 980 nm pumped UC intensity increased up to 7 mol% Er. However, the increased trend differ remarkably for the green and orange emission bands as well as under pumping energy. Under both 808 nm and 980 nm pumping, the orange emission peak monotonically increased with increasing Er concentration, even though the increase was much pronounced at 808 nm pumping (>40 fold increase, see inset in Fig.4 (a,b)). However, the increase of green peak was less pronounced under both 808 nm (~10 fold increase, see inset in Fig.4a) and 980 nm pumping (~5 fold increase, see inset in Fig.4b). Further, the green emission peak satured as early as ~3 mol% Er ions concentration but the orange emission peak was not saturated until 7 mol% Er. It is worth mentioning that the concentration quenching was started at lower concentration under 980 nm pumping compared to the 808 nm pumping. Obviously, 808 nm photons were absorbed by Er ions itself corresponding to ($^4I_{15/2}$ → $^4I_{9/2}$) electronic transition, but 980 nm was absorbed by Yb (($^2F_{7/2}$ → $^2F_{5/2}$) and energy transfer from Yb→Er generates the Er UC. It is assumed that cross relaxation from higher energy states ($^2H_{11/2}$, $^4S_{3/2}$) to lower energy states ($^4I_{9/2}$) of Er ions and Er ($^4I_{11/2}$) to Er ($^4I_{11/2}$) energy migrations were pronounced earlier under 980 nm excitation. When 808 nm laser was used, direct two step absorption followed by lattice relaxation easily populates higher energy states of Er ($^2H_{11/2}$, $^4S_{3/2}$) and concentration quenching was observed at relatively higher Er concentrations (> 7 mol% Er). However, under low energy excitation (980 nm), the phonon assisted relaxation from $^4I_{11/2}$ to the lower lying $^4I_{13/2}$ states is more pronounced, thus it is difficult to populate higher energy states ($^2H_{11/2}$, $^4S_{3/2}$) to generate green UC. The detail UC mechanism will be discussed later.

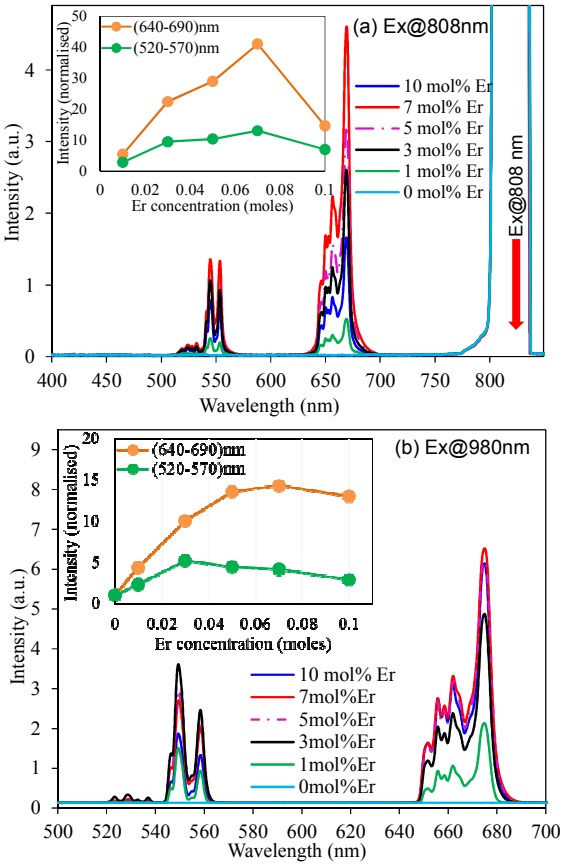

Fig. 4. UC emission profiles of Y_2BaZnO_5:x mol%Er, 7 mol% Yb phosphors: (a) Excitation at 808 nm and (b) excitation at 980 nm. Insets are the integrated intensities of green (520-570 nm) and red (640-690 nm) emissions as a function of Er ions concentration.

Figure 5 represents the effect of Yb^{3+} ions concentration at fixed 3 mol% Er ions concentration. Under 980 nm excitation, the intensities of the green emissions band gradually increased with increasing Yb^{3+} ions concentration up to 15 mol% above that it started decreasing (Fig. 5b). However, the orange emission band monotonically increased even up to 20 mol%. Completely different trend was observed when 808 nm laser was used; green band decreased with increasing Yb concentration from the beginning but orange band increased first up to 10 mol% Yb and then decreased further increasing its concentration. When direct Er is excited by 808 nm laser, with increasing Yb concentration back transfer of excited photons from $^4I_{11/2}$ (Er) to $^2F_{5/2}$ (Yb) increases which decreases the photons population at $^4I_{11/2}$ (Er) states and consequently the excitation from $^4I_{11/2}$ (Er) to higher states $^4F_{7/2}$ (Er) is supressed and decreased the green UC. On the contrary, at low Yb ions concentrations, the competetion between energy transfer from $^4I_{11/2}$ (Er) → $^2F_{5/2}$ (Yb) to internal relaxation to lower lying states ($^4I_{11/2}$ (Er) → $^4I_{13/2}$ (Er)) increases followed by upper states population ($^4I_{13/2}$→$^4F_{9/2}$) through ESU process increases the orange upconversion. But as the Yb concentration further increased beyond 10 mol%, the energy transfer from $^4I_{11/2}$ (Er) → $^2F_{5/2}$ (Yb) exceeds the internal relaxation leading to quenching of the Er upconversion. This concentration quenching effect could be explained by the energy transfer between the nearest activator to sensitizers and sensitizer to sensitizer internal relaxation. As the dopants concentration increased, the distance between dopants ions shrinks allowing non-radiative energy migration such as exchange, dipole or multi-pole interactions. Further, at higher rare ions concentrations, the solid solubility limits reached the maximum and a secondary phase appeared and hampered the UC emission.

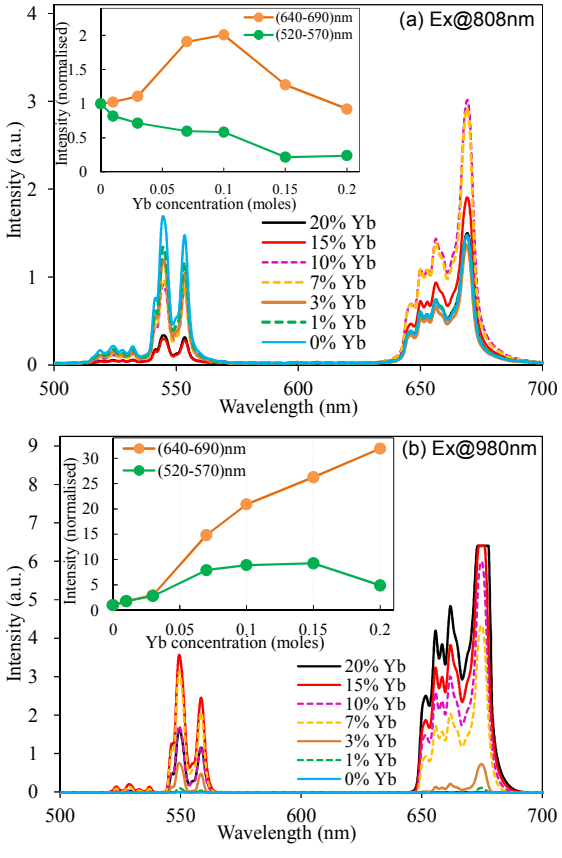

Fig. 5. UC emission profiles of Y_2BaZnO_5:3 mol%Er, x mol% Yb phosphors: (a) Excitation at 808 nm and (b) excitation at 980 nm laser. Insets are the integrated intensities of green (520-570 nm) and red (640-690 nm) emissions as a function of Yb ions concentration.

According to Judd-Ofelt theory, the partially forbidden intra 4f-4f transitions are enabled by crystal field coupling with the unoccupied electronic configurations of the rare earth ions in higher energies or with ligand to metal charge transfer configuration [35]. At low symmetry, not only the degeneracy of the free ions states removed, the transition probabilities also increased due to the overall increase in the crystal field strength. Thus, to develop highly efficient UC phosphors that utilizes the specific energy level schemes of the the rare earth ions, symmetry breaking is one of the most promising way. Use of monovalent charge compensator ions (such as Li^+, Na^+, K^+, Ag^+ *etc*) showed promising effect on the enhancement of emission intensity of the alkali or alkaline earth based materials [36–39]. S. Das *et al.* explained that the K^+ ions addition on the $CaSO_4:Dy^{3+}$ phosphor and enhanced the PL intensity significantly [40]. J.H. Chung *et al.* significantly increased the UC intensity of $CaMoO_4$ blue phosphor by excess Li^+ ions addition [41]. We have previously reported many fold improvement of UC intensity of blue, green and orange emissions in $CaMoO_4:RE^{3+}$ (Tm/Er/Ho) by alkali metal ions substitution at the divalent Ca^{2+} ions sites and explained the effect by distortion of the crystal field of RE^{3+} (Tm/Er/Ho) ions due to size and charge difference [13]. Recently, Y. Hu *et. al.* remarkably improved the red UC of $NaYF_4$:Yb,Er by Fe^{3+} and Mn^{2+} doping and explained the underlined mechanism due to crystal field and symmetry lowering around the Er ions enhancing the f-f transition probabilites [22]. However, they have used very high concentration of Fe and Mn ions that significantly altered the crystal phase. Herein, we have reported for the first time, the significant improvement of the both green and orange upconversion in oxide based phosphor using the very similar crystal field breaking and symmetry lowering technique by doping very small amount of the V^{5+} ions into the Y_2BaZnO_5:Er phosphor.

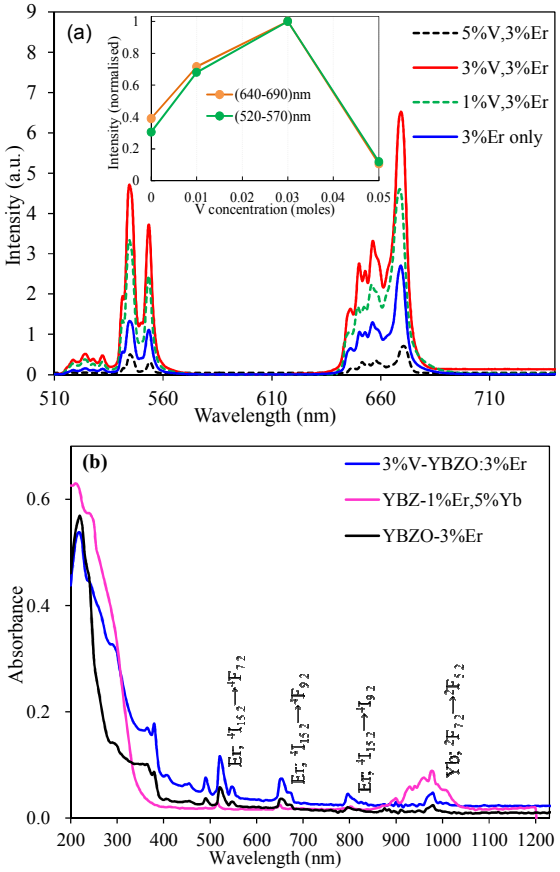

Fig. 6. UC emission profiles of Y_2BaZnO_5:3 mol% Er, x mol% V phosphors (excitation at 808 nm) and (b) absorption spectra of selected samples. Inset in Fig. 6(a) is the integrated intensities of green (520-570 nm) and red (640-690 nm) emissions as a function of V ions concentration.

Fig. 6(a) shows the effect of V^{5+} ions substitution on the green and orange emission of the Y_2BaZnO_5:3 mol%Er phosphors excited by 808 nm. Substitution of V^{5+} ions significantly intensified the UC emission intensities of both the green and orange emission bands upto 3 mol% V^{5+} ions substitution, which was more than 3 times compared to the V^{5+} ions unsubstituted sample as shown in the inset of Fig 7(a). Further increase of V^{5+} ions above 3 mol% decreased the UC intensity. We have recorded the absorption spectra of selected samples and expressed in Fig. 6(b). There was no significant absorption band related to the V^{5+} ions. However, the Er^{3+} related absorption band were improved significantly compared to the V^{5+} ions undoped sample. It confirmed that the improvement of the UC intensity was not related to the sensitization effect of the V^{5+} ions like Yb^{3+} rather it is related to the change of crystal field and its symmetry around the Er^{3+} ions due to the V^{5+} ions substitution. As seen from the XRD in Fig.7, the doping of V^{5+} ions showed significant change in the XRD peak position to higher 2θ value indicating shrinkage of lattice due to substitution of bigger Zn^{2+} (0.090 nm) sites by smaller V^{5+} (0.070 nm) sites. It suggests that the V^{5+} ions occupied the Zn sites in the host lattice. The small V^{5+} ions with higher charge density significantly distort the crystal field around the Er^{3+} ions in the Y_2BaZnO_5 matrix that cause severe crystal field break and disorder around Er^{3+} ions. This causes the redistribution of electron cloud around the Er^{3+} ions, as a consequence, the 4f-4f transition probalities of Er^{3+} ions increased and significantly increases the UC emission intensities [7,22,35,38,42,43]. However, at higher V concentrations, secondary phase was clearly observed marked by stars in the Fig.7 and hampered the UC.

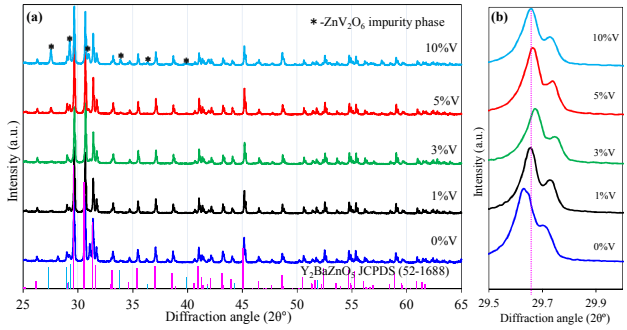

Fig. 7. (a) XRD profiles of the Y_2BaZnO_5:3 mol% Er, x mol% V phosphors and (b) portion of XRD patterns showing peak shift with V doping concentration.

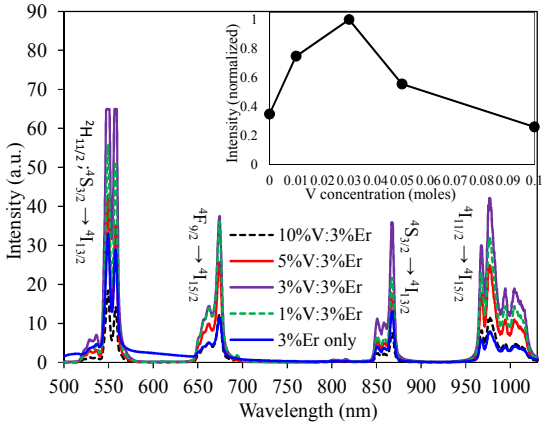

Fig. 8. PL emission profiles of Y_2BaZnO_5:3 mol% Er, x mol% V phosphors excited at 442 nm. Inset is the normalised emission intensity (integrated over 540-1030 nm) as a function of V ions concentration.

Figure 8 shows the 442 nm excited stokes emissions of Er recorded from 500 nm to 1050 nm range. Due to sufficiently strong excitation and hence population of upper excited states various $f^n \rightarrow f^n$ transitions were observed besides certain bands observed at 808 nm and 980 nm excitation. The inset of Fig. 8 shows the normalised emission intensity (integrated over whole range *viz.* 540-1030 nm) as a function of V ions concentration. The same trend was found for the variation of emission intensities with V substitution as observed while pumping at 808 nm. It further implies that all the electronic transitions of Er were intensified significantly by V-doping.

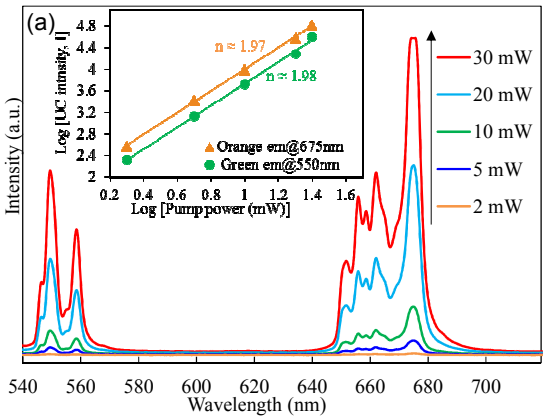

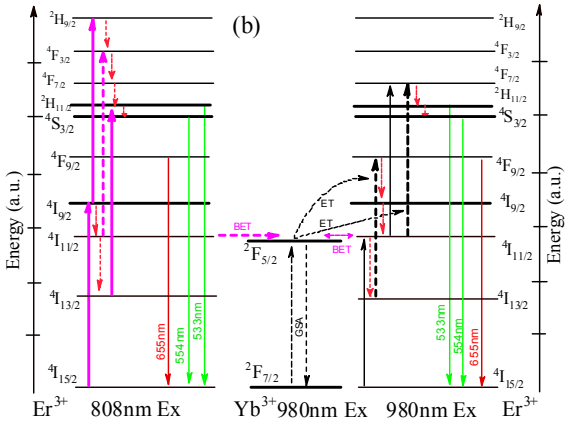

Fig. 9. (a) Pump power dependence upconversion intensity of Y_2BaZnO_5:3 mol% Er, 7 mol% Yb phosphors by 808 nm laser excitation. Inset is the n dependent UC relationship from pump power verses UC intensity and (b) Simplified energy level diagrams of $Er^{3+}(Yb^{3+})$:Y_2BaZnO_5 phosphors.

Figure 9 shows the excitation power dependence of green and orange UC emissions in the Y_2BaZnO_5:Er phosphors. It is well known that for unsaturated UC processes, the number of photons required to populate the upper lying states can be obtained by the following general equation:

$I \alpha P^n$

where n is a number of pumping photons required to excite the emitting state, I is the UC intensity and P is the laser pumping power. The calculated result (Fig. 9) indicates that the slope is ~1.96 for orange UC, 1.97 for green UC emissions. This result indicates that the green ($^2H_{11/2}/^4S_{3/2} \rightarrow ^4I_{15/2}$) and orange ($^5F_5/^5F_4/^5S_2 \rightarrow ^5I_8$) upconversion processes involves two photons upconversion processes [4,5,15,20,44].

According to above results the upconversion mechanism of Y_2BaZnO_5:Er phosphor can be generalized as in Fig. 9(b). The UC mechanism under 980 nm lasers pumping was well studied and can be seen in detail at Refs. 11 and 20. Under 808 nm lasers pumping, the $^4I_{9/2}$ state gets populated ($^4I_{15/2} \rightarrow ^4I_{9/2}$). Successive excitation (excited state absorption, ESA) of the $^4I_{9/2}$ state populates the $^2H_{9/2}$ state. From the $^2H_{9/2}$ state the excited photons relax

nonradiatively to the $^2H_{11/2}$ and then to the $^4S_{3/2}$ level, from where green emission is observed ($^2H_{11/2}/^4S_{3/2}\rightarrow{}^4I_{15/2}$; green emission). At the same time, photons from the $^4I_{9/2}$ state relax nonradiatively to the $^4I_{11/2}$ state. The lifetime of $^4I_{11/2}$ state is comparatively long [15], the energy transfer upconversion (ETU) from the nearby Er^{3+} ions populates the $^2H_{11/2}$ and then to the $^4S_{3/2}$ levels through the nonradiative relaxation from higher $^4F_{3/2}$ and $^4F_{7/2}$ states and radiative transition from the $^2H_{11/2}/^4S_{3/2}$ levels gives the prominent green emission ($^2H_{11/2}/^4S_{3/2}\rightarrow{}^4I_{15/2}$). The non radiative relaxation from the $^4S_{3/2}$ state to the low lying $^4F_{9/2}$ state or radiative relaxation from the ($^4F_{3/2}/^4F_{7/2}$) to the $^4F_{9/2}$, populates the $^4F_{9/2}$ state, from where transition to the ground state ($^4I_{15/2}$) generates the red UC ($^4F_{9/2}\rightarrow{}^4I_{15/2}$; red emission). Here, important point is that when Er concentration was high enough, ETU dominates, which populates only $^4F_{9/2}$ states as a consequence, the red UC will be prominent. It means, the quenching concentration of the red UC is comparatively larger than the green UC due to competetion between ETU and ESA at higher Er concentration. It can be further supported by the indirect 980 nm pumping through Yb^{3+} ions. When 980 nm laser is used, the $^2F_{5/2}$ states of Yb^{3+} gets populated. Then non-resonant energy transfer from the $^2F_{5/2}$ (of Yb^{3+}) level to the $^4I_{11/2}$ level of Er^{3+} populates the $^4I_{11/2}$ level. Nonradiative relaxation to the $^4I_{13/2}$ level followed by ETU populates the $^4F_{9/2}$ states to generate red UC. At the same time, due to long life time of the $^4I_{11/2}$ state, the $^2H_{11/2}$ and $^4S_{3/2}$ states get populated partially through nonradiative relaxation from $^4F_{7/2}$. Thus, excited state population of the $^2H_{11/2}$ and $^4S_{3/2}$ states are comparatively low than the population of the $^4F_{9/2}$ states while pumping at 980 nm, which is seen as strong red and weak green UC at 980 nm pumping but strong green and weak red UC at stronger (808 & 442) nm pumping.

4. Conclusion

A facile hydrothermal procedure was used to synthesize microcapsules of $Y_2BaZnO_5:Er^{3+}$ upconversion phosphor. Spherical balls of 1-5 μm size and hollow architectures of about 50 nm shell wall were fabricated by HT treatment and these microcapsules were stable even at high temperature of 1000 ℃. The underlined microcapsule formation mechanism was discussed using gas-bubble-assisted Ostwald ripening process. Yellowish green UC emissions were achieved by pumping with 808 as well as 980 nm lasers. The optimum Er^{3+} doped concentration for 550 nm and 660 nm UC luminescence intensities were 5 mol% and 7 mol%, respectively. In addition, the optimum Er concentration differed from the excitation wavelength indicating different mechanism under 808 and 980 nm pumping. Importantly, optimum amount of the V^{5+} co-doping into the $Y_2BaZnO_5:Er^{3+}$ phosphors intensified the UC intensity by more than 3 fold. The redistribution of electron cloud around the Er^{3+} ions by crystal field distortion and symmetry lowering of the crystal after introducing V^{5+} was suggested to be the origin of the UC improvement. The $Y_2BaZnO_5:Er^{3+},V^{5+}$ phosphor exhibited very intense yellowish UC pumped by 808 nm laser and will have potential applications for the in vivo biological labelling, biomedical imaging and therapies.

Notes and references

Department of Advanced Technology Fusion, Saga University, Honjo-1, Saga, 850-8502, Japan.
[*]*mehomnath@yahoo.com (Hom Nath Luitel)*
[#]*watarit@cc.saga-u.ac.jp (Takanori Watari)*
Tel.: +81 952 28 8683
Fax: +81 952 28 8548

[1] J. Wang, P.A. Tanner, J. Am. Chem. Soc. 132 (2010) 947–949.
[2] J. Zhou, Q. Liu, W. Feng, Y. Sun, F. Li, Chem. Rev. 115 (2015) 395–465.
[3] X. Huang, S. Han, W. Huang, X. Liu, Chem. Soc. Rev. 42 (2013) 173-201.
[4] X. Li, F. Zhang, D. Zhao, Chem. Soc. Rev. 44 (2015) 1346–1378.
[5] W. Kaiser, C. Garrett, Phys. Rev. Lett. 7 (1961) 229–231.
[6] P. Du, Z. Xia, L. Liao, Adv. Mater. Sci. Eng. vol. 2015 (2015) 5 pages.
[7] B. Zhou, B. Shi, D. Jin, X. Liu, Nat. Nanotechnol. 10 (2015) 924–936.
[8] L. Hesselink, J. Ralston, R. Macfarlane, Science 273 (1996) 1185.
[9] Q. Zhang, G. Chen, G. Zhang, J. Qiu, D. Chen, J. Appl. Phys. 133 (2010) 034507.
[10] B.P. Singh, A.K. Parchur, R.K. Singh et.al., Phys. Chem. Chem. Phys. Phys. Chem. Chem. Phys. 15 (2013) 3480–3489.
[11] H.N. Luitel, K. Ikeue, R. Okuda, R. Chand, T. Torikai, M. Yada, T. Watari, Opt. Mater. 36 (2014) 591–595.
[12] Y. Min, J. Li, F. Liu, P. Padmanabhan, E. Yeow, B. Xing, Nanomaterials. 4 (2014) 129–154.
[13] H.N. Luitel, R. Chand, T. Torikai, M. Yada, T. Watari, RSC Adv. 5 (2015) 17034.
[14] I. Etchart, A. Huignard, M.B. Erard, M.N. Nordin, I. Hern Andez, R.J. Curry, et al., J. Mater. Chem. 20 (2010) 3989–3994.
[15] A. Lupei, V. Lupei, C. Gheorghe, A. Ikesue, E. Osiac, Opt. Mater. 31 (2009) 744–749.
[16] C. Strümpel, M. McCann, G. Beaucarne et al., Sol. Energy Mater. Sol. Cells. 91 (2007) 238–249.
[17] Y. Zhou, X.H. He, B. Yan, Opt. Mater. 36 (2014) 602–607.
[18] N.C. Dyck, F.C.J.M. Van Veggel, G.P. Demopoulos, ACS Appl. Mater. Interfaces 5 (2013) 11661–11667.
[19] J. de Wild, A. Meijerink, J.K. Rath, W.G.J.H.M. van Sark, R.E.I. Schropp, Energy Environ. Sci. 4 (2011) 4835.
[20] M. Pokhrel, A.K. Gangadharan, D.K. Sardar, Mater. Lett. 99 (2013) 86–89.
[21] X. Shang, P. Chen, T. Jia, D. Feng, S. Zhang, Z. Sun, et al., Phys. Chem. Chem. Phys. 17 (2015) 11481–11489.
[22] Y. Hu, X. Liang, Y. Wang, E. Liu, X. Hu, J. Fan, Ceram. Int. 41 (2015) 14545–14553.
[23] Ralph Weissleder, Nat. Biotechnol. 19 (2001) 316–317.
[24] D. Adikaari, I. Etchart, P.H. Guéring, M. Bérard, S.R.P. Silva, A.K. Cheetham, et al., J. Appl. Phys. 111 (2012) 094502.
[25] C. Li, J. Lin, J. Mater. Chem. 20 (2010) 6831.
[26] M.C. Tan, L. Al-Baroudi, R.E. Riman, ACS Appl. Mater. Interfaces. 3 (2011) 3910–3915.
[27] B. Xue, J. Sun, INFRARED Phys. Technol. 62 (2014) 45–49.
[28] E.D. Sternberg, D. Dolphin, C. Brickner, Tetrahedron. 54 (1998) 4151–4202.
[29] http://abulafia.mt.ic.ac.uk/shannon/ptable.php.
[30]X. Liu, Y. Li, W. Zhu, P. Fu, CrystEngComm 15 (2013) 4937–4947.
[31] C. Cao, Z. Cui, C. Chen, W. Song, W. Cai, J. Phys. Chem. C 114 (2010) 9865–9870.
[32] S. Cho, J. Jang, S. Jung, B.R. Lee, E. Oh, K. Lee, Langmuir 25 (2009) 3825–3831.
[33] G. Xue, X. Huang, N. Zhao, F. Xiao, W. Wei, RSC Adv. 5 (2015) 13385–13391.
[34] H.N. Luitel, R. Chand, T. Torikai, M. Yada, T. Watari, Inter. J. Photoenergy, 2013 (2013) article id 40613.
[35] M.F. Reid, Crystal field handbook, Cambridge Univ. press, 2000.
[36] H.N. Luitel, T. Watari, R. Chand, T. Torikai, M. Yada, J. Mater. 2013 (2013) article id 613090.
[37] S. Das, A. Amarnath Reddy, G. Vijaya Prakash, Ceram. Int. 38 (2012) 5769-5773.
[38] S. Dutta, S. Som, S.K. Sharma, Dalton Trans. 42 (2013) 9654–9661.
[39] H.N. Luitel, R. Chand, T. Watari, Displays 42 (2016) 1-8.
[40] S. Das, A. Amarnath Reddy, G. Vijaya Prakash, Ceram. Int. 38 (2012) 5769–5773.
[41] J. Ho, C. Sang, Y. Lee, Kwang, B. Shim, S.-Y. Kweon, et al., Appl. Phys. A. 108 (2012) 369–373.
[42] B.S. Cao, Y.Y. He, L. Zhang, B. Dong, J. Lumin. 135 (2013) 128–132.
[43] F. Wang, Y. Han, C.S. Lim, Y. Lu, J. Wang, J. Xu, et al., Nature 463 (2010) 1061–1065.

[44] L. Liu, H. Jiang, Y. Chen, X. Zhang, Z. Zhang, Y. Wang, J. Lumin. 143 (2013) 423–431.

Graphical Abstract

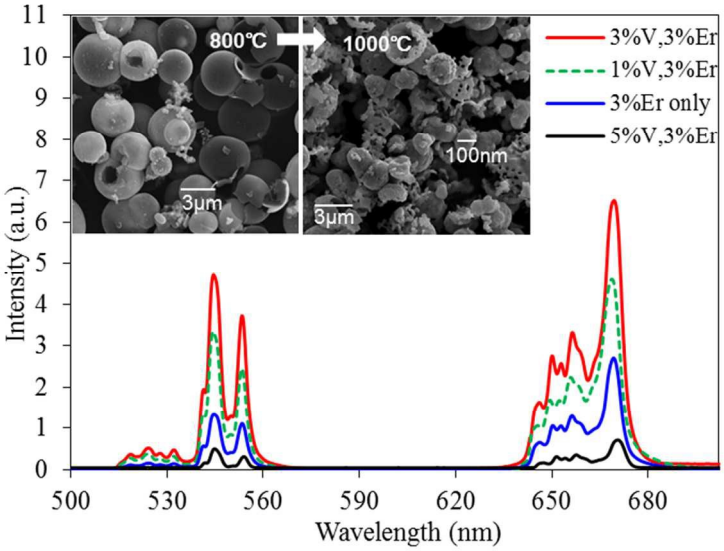

$Er^{3+}/V^{5+}/Yb^{3+}$ doped Y_2BaZnO_5 microcapsules (hollow spheres) of 1-3 μm were prepared by simple HT route using citric acid and urea. Bright green to orange UC was observed by dual 800 nm and 980 nm laser excitation. More than 3 fold intensification of Er UC was achieved by 3 mol% V^{5+} substitution at the Zn sites which is ascribed to the change in crystal field around Er^{3+} ions.